Ø. Hammer, S.E. Lauritzen, and B. Jamtveit – Stability of dissolution flutes under turbulent flow. *Journal of Cave and Karst Studies,* v. 73, no. 3, p. 181–186. DOI: 10.4311/2011JCKS0200

STABILITY OF DISSOLUTION FLUTES UNDER TURBULENT FLOW

ØYVIND HAMMER[1*], STEIN E. LAURITZEN[2], AND BJØRN JAMTVEIT[1]

Abstract: Dissolution of a solid surface under turbulent fluid flow can lead to the formation of periodic ripple-like structures with a wavelength dependent upon flow velocity. A model coupling hydrodynamics with mass transport and dissolution kinetics shows that the shape stability of these structures can be explained from fundamental principles. The effects of a subgrid diffusion boundary layer must be included in the dissolution model to produce realistic results. The importance of including not only the mean flow velocity, but also the turbulent component of flow, in the dissolution model is emphasized. The numerical experiments also compare dissolution profiles for gypsum and calcite.

INTRODUCTION

Limestone dissolution under turbulent, high-velocity flow commonly leads to a certain surface roughness morphology known as scallops. Such scallops can have complex, three-dimensional shapes, but can also take the form of ripples or flutes oriented normal to the flow direction (Curl, 1966, 1974; Goodchild and Ford, 1971; Blumberg and Curl, 1974; Thomas, 1979; Gale, 1984; Villien, et al. 2005).

One of the most interesting properties of dissolution flutes is that their profiles are stable in time, while migrating both vertically as the surface is globally dissolved and in the downstream direction in a soliton-like manner (Blumberg and Curl, 1974). Such behavior is maintained as long as the flute with profile $y(x,t)$ obeys the one-dimensional transport equation with horizontal velocity v_x and an added term v_y for the mean dissolution rate (corresponding to vertical displacement velocity):

$$\frac{\partial y}{\partial t} = -v_x \frac{\partial y}{\partial x} - v_y. \quad (1)$$

This equation refers to dissolution rates in the vertical direction, and x is the horizontal (i.e., not tangential to the profile). The free parameters v_x and v_y allow for a family of possible dissolution profiles all compatible with a given flute shape. These parameters also imply a certain angle of translation of the flute with respect to the horizontal, as $\tan\theta = v_y / v_x$.

The dissolution rate in a direction normal to the surface can be calculated geometrically as (cf. Curl 1966, eq. 15)

$$\frac{\partial y'}{\partial t} = \frac{\frac{\partial y}{\partial t}}{\sqrt{1+\left(\frac{\partial y}{\partial x}\right)^2}} = \frac{-v_x \frac{\partial y}{\partial x} - v_y}{\sqrt{1+\left(\frac{\partial y}{\partial x}\right)^2}}. \quad (2)$$

Curl (1966) and Blumberg and Curl (1974) provided careful theoretical analysis and experimental results on dissolution scallops and flutes in gypsum. They found that the Reynolds number calculated from flute wavelength and main-channel maximum velocity remained fairly constant at Re = 23300 over a large range of flow velocities, implying an inverse relationship between flow velocity and flute wavelength. Bird et al. (2009) presented a full 3D fluid-dynamics simulation of flow over static dissolution scallops, confirming several of the observations of flow patterns described by Blumberg and Curl (1974). A recent review of dissolution scallops was given by Meakin and Jamtveit (2010).

The purpose of this paper is to couple a simple 2D fluid dynamics model to a dissolution model, and to compare the simulation dissolution profiles with the dissolution profiles required for the stability of experimental flute shapes.

METHODS

The numerical experiments all use a fixed two-dimensional flute geometry reported from laboratory experiments with gypsum at Re = 23300, flute wavelength 5.1 cm (Blumberg and Curl 1974). The empirical sine series of flute geometry normalized to flute wavelength is

$$\hat{Y} = 0.112\sin\pi\hat{X} + 0.028\sin2\pi\hat{X} - 0.004\sin3\pi\hat{X}. \quad (3)$$

To reduce boundary effects, hydrodynamics were simulated using three consecutive flutes, and subsequent study concentrated on the central flute. The total simulated area was 15.24 by 5.08 cm. A grid size of 612 by 204 gave a resolution of h = 0.25 mm. The Navier-Stokes code NaSt2D-2.0 (Griebel et al. 1997; Bauerfeind, 2006) was used with a k-ε turbulence model. In addition to the mean velocity vector field **u**, this code also produces the eddy (turbulent) viscosity v_t that can be regarded as a measure of

* Corresponding Author
[1] Physics of Geological Processes, University of Oslo, PO Box 1048 Blindern, 0316 Oslo, Norway
[2] Department of Earth Science, University of Bergen, Allegaten 41, 5007 Bergen, Norway

degree of local turbulence (Boussinesq approximation). The results of the computational fluid dynamics were cross-validated using the k-ε turbulence model provided in an independent finite volume, unstructured mesh code, OpenFoam version 1.6 (www.openfoam.com). The velocity and eddy viscosity fields given by the two programs were practically identical.

The equations for scalar transport of dissolved species were approximated using explicit finite difference methods. The advection term was implemented with a second-order Lax-Wendroff difference scheme (Lax and Wendroff, 1960). Turbulent mixing was approximated using the Reynolds analogy, where mixing is modeled as diffusion with a turbulent (eddy) diffusivity that can be orders of magnitude larger than molecular diffusivity. The turbulent diffusivity is defined as

$$\Gamma = \frac{v_t}{\sigma_t}, \tag{4}$$

where v_t is turbulent viscosity and σ_t is the turbulent Prandtl number. We used $\sigma_t = 1.0$. The complete transport equation for the concentration c with mean velocity field $\mathbf{u}$ becomes

$$\frac{\partial c}{\partial t} = -\mathbf{u}\cdot\nabla c + \nabla\cdot(\Gamma\nabla c). \tag{5}$$

Precipitation and dissolution rates under flow can be largely dependent upon the thickness of a diffusive boundary layer (e.g., Buhmann and Dreybrodt 1985; Liu and Dreybrodt 1997; Opdyke et al., 1987). The diffusive boundary layer can be only a few micrometers thick at high flow rates and is not captured with the grid size used here. For example, Curl (1966) reports a transfer coefficient $k = 3.4 \times 10^{-3}$ cm s^{-1} under conditions typical for flute formation. With a molecular diffusion coefficient of $D = 1.2 \times 10^{-5}$ cm^2 s^{-1}, this corresponds to a diffusive boundary layer thickness $\varepsilon = 35$ μm. The thickness of the diffusive boundary layer can be defined as the point where molecular and turbulent diffusivities are equal. With y the perpendicular distance from the solid-liquid interface into the liquid, molecular diffusion dominates in the region $y < \varepsilon$. With D the molecular diffusivity, we then have

$$\Gamma(\varepsilon) = \frac{v_t(\varepsilon)}{\sigma_t} = D. \tag{6}$$

Away from the boundary the eddy viscosity v_t (y') is nearly linear, vanishing near the boundary (Kleinstein, 1967). This is in accordance with the eddy viscosity profile seen from the NaSt2D-2.0 solution down to the first liquid cell over the boundary ($y' = 250$ μm). Near the boundary, the eddy viscosity profile becomes more complex and generally follows a power law with 3 as exponent (Kleinstein, 1967). However, this nonlinearity is expected to be found in a layer much thinner than the grid size. We therefore roughly estimate the subgrid values of the eddy viscosity v_t (y') by linear interpolation between the surface (v_t (0) = 0) and the prescribed value in the first cell. The thickness ε of the diffusive boundary layer can then be computed from Equation (6).

An alternative estimation of the diffusive boundary layer thickness is based on the viscous boundary layer thickness, which is much larger. The viscous boundary layer thickness δ can be defined as the height where turbulent diffusivity is equal to kinematic viscosity v and can be estimated by linear interpolation of turbulent diffusivity from the first grid cell to the interface, as above. The diffusive boundary layer thickness is then estimated using an empirical relation

$$\varepsilon = \frac{\delta}{\sigma^{\alpha}}, \tag{7}$$

where $\sigma = \upsilon D$ is the Schmidt number. The exponent α is assumed to be between 1/3 and 1/4 (Wüest and Lorke 2003). With $\sigma \approx 10^3$ and $Sc \approx 1/3$, we have $\varepsilon \approx 0.1\delta$.

The molar dissolution rate of gypsum follows the rate law of Opdyke et al. (1987):

$$R = \frac{D}{\varepsilon}\left(\left[\mathrm{Ca}^{2+}_{\mathrm{eq}}\right] - \left[\mathrm{Ca}^{2+}\right]\right), \tag{8}$$

where $\left[Ca^{2+}_{eq}\right]$ is the equilibrium concentration of 15.4 mM at 20 °C. A more complex, second-order equation was given by Raines and Dewers (1997) and Villien et al. (2005). This reaction adds calcium to the solution, modifying the boundary condition of Equation (5) at the solid-water interface. The transport equations are applied to calcium concentration only. Because the fluid dynamics are many magnitudes faster than the rate of movement of the interface due to dissolution, we run the fluid dynamics in a static geometry, where the boundary conditions are not moving.

Dissolution of calcite uses the method described by Hammer et al. (2008) with the rate equation of Plummer et al. (1978). This requires the modeling of reaction and transport of three species in solution, [CO_2], [Ca^{2+}] and the sum of the carbonate and bicarbonate concentrations $[\mathrm{c}] = \left[\mathrm{HCO}_3^-\right] + \left[\mathrm{CO}_3^{2-}\right]$. The Plummer et al. (1978) rate computed from the concentrations in the fluid cell above the interface is multiplied with an approximate empirical function of the diffusive boundary layer thickness ε, derived from Table 2 in Liu and Dreybrodt (1997):

$$b = 0.02 + \frac{0.001}{\varepsilon + 0.001}. \tag{9}$$

The transport equations use cyclic boundary conditions at the inflow and outflow boundaries. In order to keep the system away from equilibrium, maintaining dissolution over time, a sink for the dissolved species was provided by setting the concentrations to zero at the upper boundary of the domain. For the calcite model, [CO_2] was set to 0.1 mM at the upper boundary.

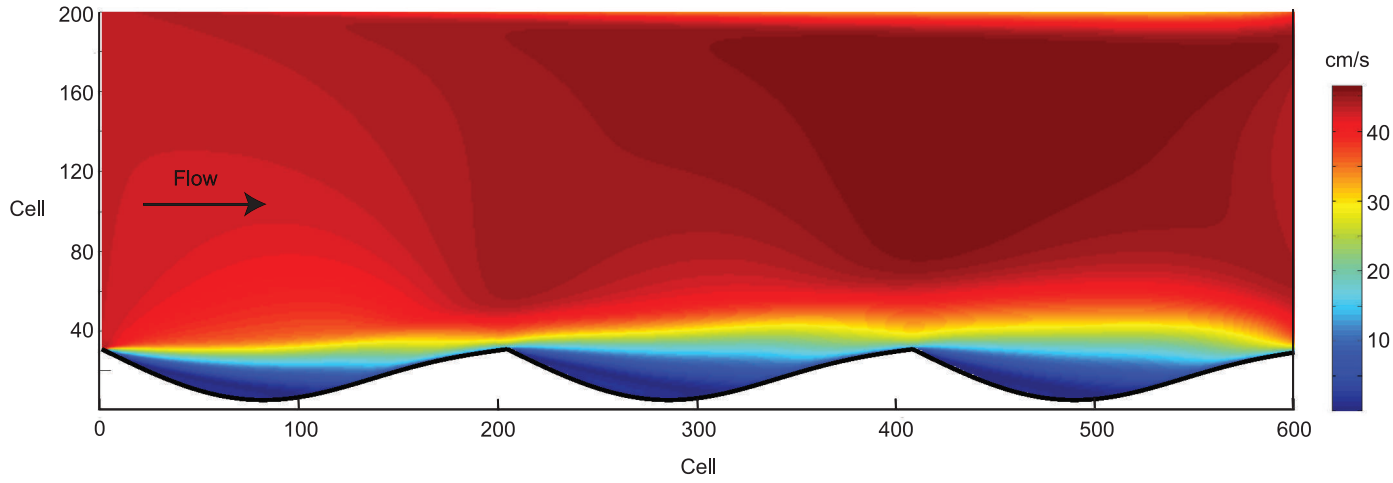

Figure 1. The geometry of the simulation, with the absolute value of mean-field flow velocity (cm/s). Flow from left to right.

Results

The model geometry and mean flow velocity are shown in Figure 1. The flow streamlines in Figure 2 demonstrate flow separation at the crest and the formation of a back eddy. The flow reattachment point is found near the lower end of the stoss side, while the region of maximal eddy viscosity is localized further up the slope. The mean velocity profile away from the fluted wall is precisely logarithmic up to a distance of about 1 cm, after which it starts to diverge from logarithmic towards the middle of the channel due to the inflow and outflow boundary conditions.

Figure 3 shows the Ca concentration field from the dissolution of gypsum, and the simulated dissolution profile together with a theoretical profile (rate normal to the surface) calculated from Equations (2) and (3). Apart from a ragged appearance due to the discretization grid, the simulation result is similar to the theoretical profile, with a sharp decrease in dissolution rate after the crest followed by a gradual increase to a maximum about halfway up the stoss side. However, the recovery of dissolution rate downstream from the crest is somewhat delayed in the simulation compared with the theoretical profile.

To assess the sensitivity to grid resolution, the complete simulation (fluid dynamics, transport and dissolution) was repeated on a twice coarser grid (306 by 102, $h = 0.5$ mm), and also with a 1 mm grid. The dissolution profiles were indistinguishable in shape between these runs, but overall dissolution rate scaled with roughly the square root of h. We ascribe this scale difference to the decrease as cell size increases in average concentration of dissolved species in the first cell over the interface. However, since the shape of the profile is unaffected, this grid dependence does not influence conclusions about the stability of the flutes.

The calcite dissolution profile (Fig. 4) seems further removed from the ideal profile than for the gypsum case, with a more gentle decrease in dissolution rate after the crest and without a clear maximum on the stoss side. Another difference between the two simulations is the smaller amplitude of the dissolution profile compared with the average value for calcite than for gypsum. This implies a larger k/v_x value for calcite, and therefore, a larger angle of flute translation with respect to the horizontal. Using the

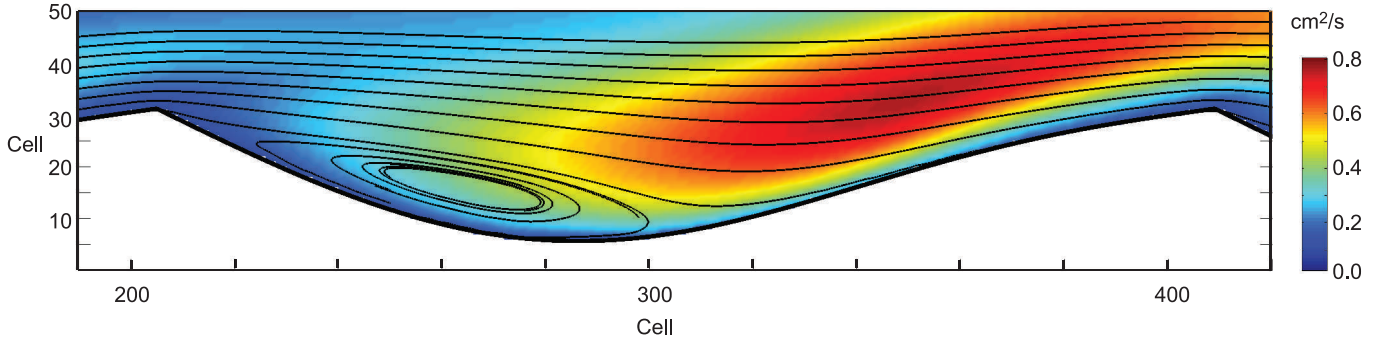

Figure 2. The central part of the modeled domain, with mean-field flow streamlines (black). The eddy viscosity field (colors) indicates degree of local turbulence.

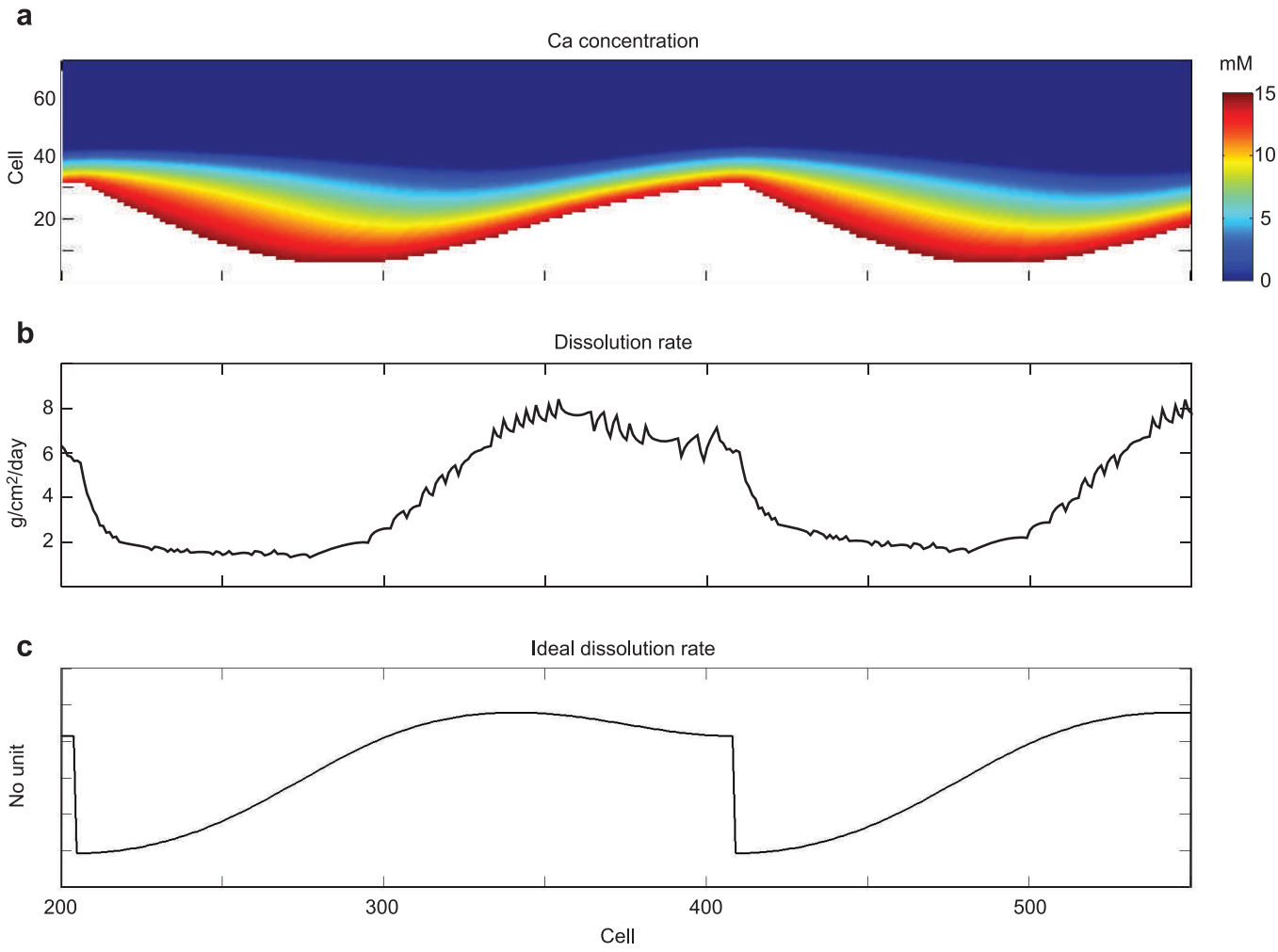

Figure 3. Results from simulation coupling hydrodynamics with gypsum dissolution. a: Calcium concentration in solution (mM). b: Simulated dissolution rate profile, aligned with fig. 3a. c: Theoretical dissolution profile for stable flutes, calculated from Equations 2 and 3.

ratio between mean dissolution rates in the horizontal and vertical directions, the angle at which the flute moves into the dissolving face can be computed as about 54 degrees for the gypsum simulation, compared with the 61 ± 2 degrees reported by Blumberg and Curl (1974) and 80 degrees for the calcite simulation. These differences can only be due to the different equations used for dissolution kinetics, possibly indicating that the rate equation of Plummer et al. (1978) or Equation (9) above is not fully applicable under the conditions simulated here.

The correspondence between ideal and modeled dissolution curve can be illustrated by plotting the $\partial y/\partial t$ from the simulation against $\partial y/\partial x$. According to Equation (1), this relationship should be linear, with slope $-v_x$. By setting $-v_y$ equal to the average dissolution rate from the simulation, the ideal slope can be calculated as $-v_x = v_y/\tan\theta$. As shown in Figure 5 for the gypsum case, the displacement of the dissolution profile downstream of the crest compared to the theoretical case gives too low slope of a on the lee side of the trough, overcompensating for an excessive slope on the stoss side. Near the bottom of the trough and near the top of the crest, the data follow a more linear trend.

DISCUSSION

The simple model described above seems sufficient to capture the essential aspects of the stability of dissolution flutes. The inclusion of turbulent mixing and the thinning of the laminar boundary layer under turbulence are necessary for reproducing a dissolution maximum close to the predicted position. The displacement of the dissolution maximum from the reattachment point and closer to the position of maximum eddy viscosity may indicate that dissolution in this region is controlled more by turbulence effects than by the angle of flow with respect to the surface, as suggested by Bird et al. (2009). On the other hand, the underestimation of dissolution rate near the reattachment point may indicate that the balance between the influence

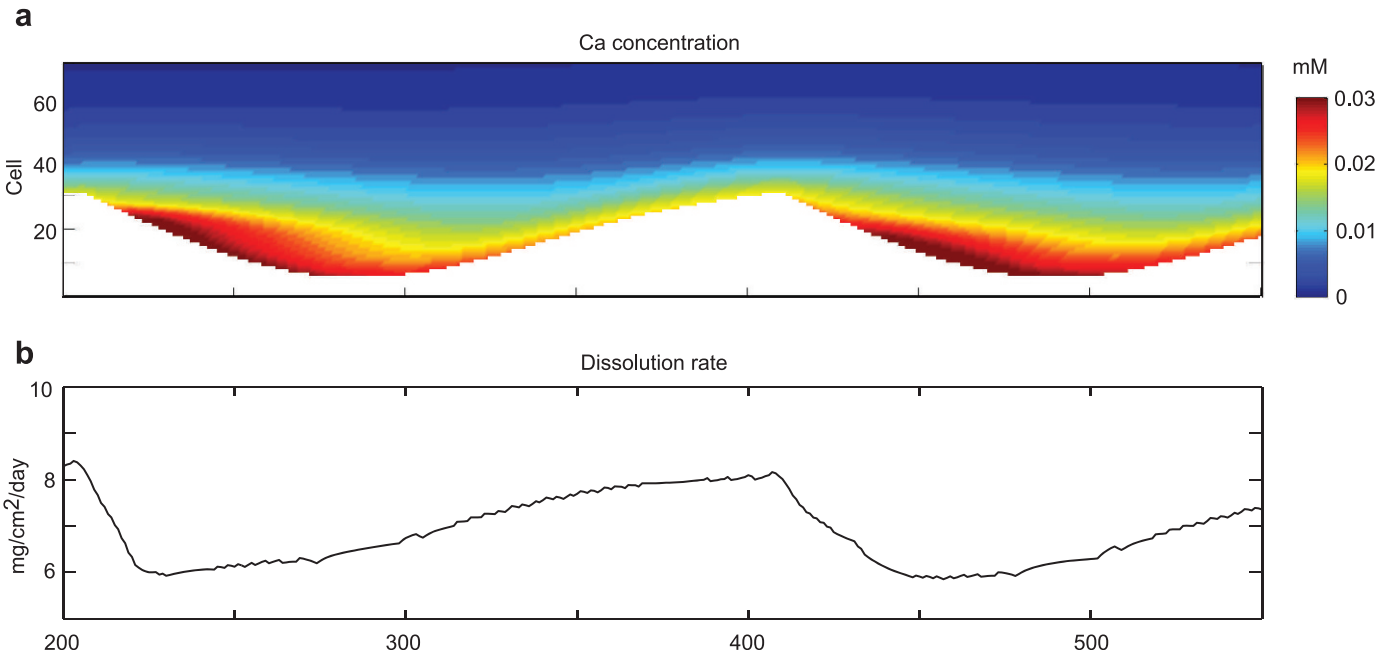

Figure 4. Results from simulation coupling hydrodynamics with calcite dissolution. a: Calcium concentration in solution. b: Simulated dissolution rate profile.

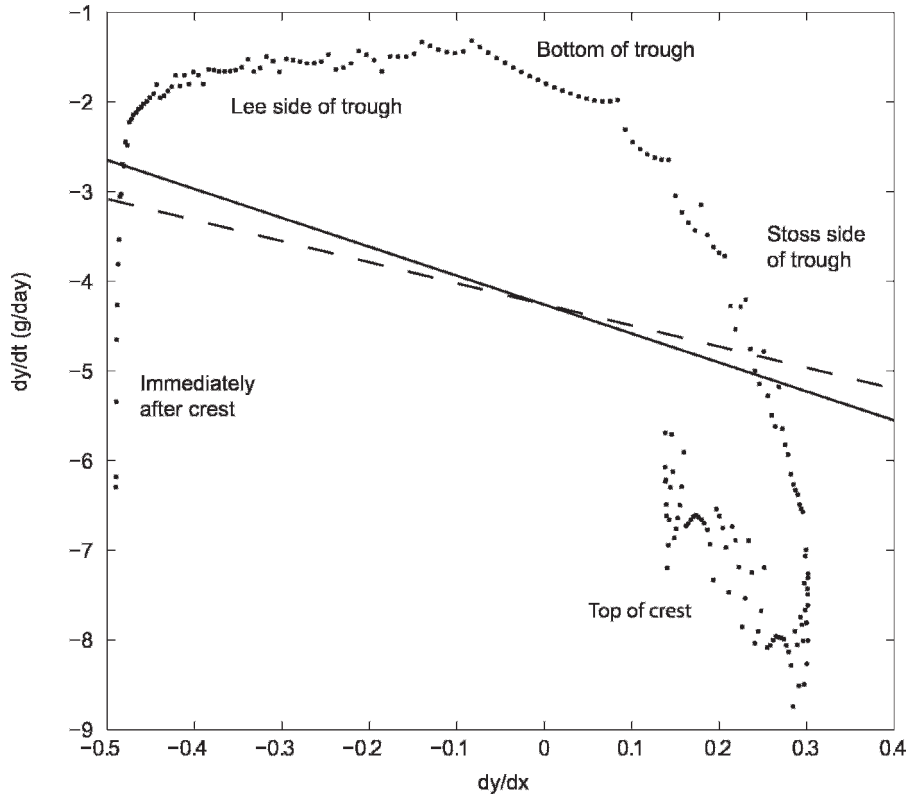

Figure 5. A plot of the result from the gypsum dissolution model, cf Equation (1) in text. Local slope of the flute profile ($\partial y/\partial x$) versus velocity of surface dissolution in the vertical direction ($\partial y/\partial t$). Dashed line: Theoretical relationship for stable flutes based on the experimental dissolution angle of 61° (Blumberg and Curl, 1974). Solid line: Theoretical relationship based on the angle of 54° resulting from the simulation.

of mean flow advection and turbulence needs further tuning to reproduce the theoretical result. More advanced turbulence modeling (including the simulation of unsteady turbulence by, for example, large eddy simulation) and also improved empirical or theoretical models for dissolution kinetics may prove useful in this respect. The exact profile of eddy viscosity very close to the solid-fluid interface (here assumed linear), which influences the estimation of diffusive boundary layer thickness, may also be a factor.

The poorer results of the calcite model compared to the gypsum model are interesting. The only difference between the two simulations is in the dissolution kinetics. It is possible that the different solution and dissolution kinetics of the calcite system would lead to a different stable flute shape than for the gypsum system, and that the gypsum flute geometry used in the simulation does not represent the steady state for calcite. However, the calcite flute shapes illustrated by Curl (1966; Fig. 3) do not appear very different from the gypsum flutes. It is therefore possible that the calcite dissolution model used here does not fully reflect the kinetics in the natural system.

ACKNOWLEDGEMENTS

Thanks to Luiza Angheluta and two anonymous reviewers for useful comments on the manuscript.

This study was supported by a Center of Excellence grant to PGP from the Norwegian Research Council.

REFERENCES

Bauerfeind, K., 2006, Fluid Dynamic Computations with NaSt2D-2.0, Open-source Navier-Stokes solver, http://home.arcor.de/drklaus.bauerfeind/nast/eNaSt2D.html [accessed February 28, 2011].

Bird, A.J., Springer, G.S., Bosch, R.F., and Curl, R.L., 2009, Effects of surface morphologies on flow behavior in karst conduits, *in* Proceedings, 15th International Congress of Speleology: Kerrville, Texas, National Speleological Society, p. 1417–1421.

Blumberg, P.N., and Curl, R.L., 1974, Experimental and theoretical studies of dissolution roughness: Journal of Fluid Mechanics, v. 65, p. 735–751. doi:10.1017/S0022112074001625.

Buhmann, D., and Dreybrodt, W., 1985, The kinetics of calcite dissolution and precipitation in geologically relevant situations of karst areas. 1. Open system: Chemical Geology, v. 48, p. 189–211. doi:10.1016/0009-2541(85)90046-4.

Curl, R.L., 1966, Scallops and flutes: Transactions of Cave Research Group of Great Britain, v. 7, p. 121–160.

Curl, R.L., 1974, Deducing flow velocity in cave conduits from scallops: National Speological Society Bulletin, v. 36, p. 1–5.

Gale, S., 1984, The hydraulics of conduit flow in carbonate aquifers: Journal of Hydrology, v. 70, p. 309–327. doi:10.1016/0022-1694(84)90129-X.

Goodchild, M.F., and Ford, D.C., 1971, Analysis of scallop patterns by simulation under controlled conditions: Journal of Geology, v. 79, p. 52–62.

Griebel, M., Dornseider, T., and Neunhoeffer, T., 1997, Numerical Simulation in Fluid Dynamics: A Practical Application (SIAM monographs on mathematical modeling and computation 3), Philadelphia, Society for Industrial and Applied Mathematics, 217 p.

Hammer, Ø., Dysthe, D.K., Lelu, B., Lund, H., Meakin, P., and Jamtveit, B., 2008, Calcite precipitation instability under laminar, open-channel flow: Geochimica et Cosmochimica Acta, v. 72, p. 5009–5021. doi:10.1016/j.gca.2008.07.028.

Kleinstein, G., 1967, Generalized law of the wall and eddy viscosity model for wall boundary layers: American Institute of Aeronautics and Astronautics Journal, v. 5, p. 1402–1407.

Lax, P.D., and Wendroff, B., 1960, Systems of conservation laws: Communications on Pure and Applied Mathematics, v. 13, p. 217–237. doi: 10.1002/cpa.3160130205.

Liu, Z., and Dreybrodt, W., 1997, Dissolution kinetics of calcium carbonate minerals in H_2O–CO_2 solutions in turbulent flow: The role of the diffusion boundary layer and the slow reaction $H_2O + CO_2 \leftrightarrows HCO_3^-$: Geochimica and Cosmochimica Acta, v. 61, p. 2879–2889. doi 10.1016/S0016-7037(97)00143-9.

Meakin, P., and Jamtveit, B., 2010, Geological pattern formation by growth and dissolution in aqueous systems: Proceedings of the Royal Society of London A, v. 466, p. 659–694. doi: 10.1098/rspa.2009.0189.

Opdyke, B.N., Gust, G., and Ledwell, J.R., 1987, Mass transfer from smooth alabaster surfaces in turbulent flows: Geophysical Research Letters, v. 14, p. 1131–1134. doi:10.1029/GL014i011p01131.

Plummer, L.N., Wigley, T.M.L., and Parkhurst, D.L., 1978, The kinetics of calcite dissolution in CO_2-water systems at 5 degrees to 60 degrees C and 0.0 to 1.0 atm CO_2: American Journal of Science, v. 278, p. 179–216. doi: 10.2475/ajs.278.2.179.

Raines, M.A., and Dewers, T.A., 1997, Mixed transport/reaction control of gypsum dissolution kinetics in aqueous solutions and initiation of gypsum karst: Chemical Geology, v. 140, p. 29–48. doi:10.1016/S0009-2541(97)00018-1.

Thomas, R.M., 1979, Size of scallops and ripples formed by flowing water: Nature, v. 277, p. 281–283. doi:10.1038/277281a0.

Villien, B., Zheng, Y., and Lister, D., 2005, Surface dissolution and the development of scallops: Chemical Engineering Communications, v. 192, p. 125–136. doi: 10.1080/00986440590473272.

Wüest, A., and Lorke, A., 2003, Small-scale hydrodynamics in lakes: Annual Review of Fluid Dynamics, v. 35, p. 373–412. doi: 10.1146/annurev.fluid.35.101101.161220.